INSTITUTE OF PHYSICS PUBLISHING PHYSIOLOGICAL MEASUREMENT

Physiol. Meas. **26** (2005) 1059–1073 doi:10.1088/0967-3334/26/6/015

# Artifact reduction in magnetogastrography using fast independent component analysis

**Andrei Irimia and L Alan Bradshaw**

Living State Physics Laboratories, Department of Physics and Astronomy, Vanderbilt University, Nashville, TN 37235, USA

E-mail: andrei.irimia@vanderbilt.edu

Received 10 August 2005, accepted for publication 21 September 2005
Published 7 November 2005
Online at stacks.iop.org/PM/26/1059

**Abstract**

The analysis of magnetogastrographic (MGG) signals has been limited to epochs of data with limited interference from extraneous signal components that are often present and may even dominate MGG data. Such artifacts can be of both biological (cardiac, intestinal and muscular activities, motion artifacts, etc) and non-biological (environmental noise) origin. Conventional methods—such as Butterworth and Tchebyshev filters—can be of great use, but there are many disadvantages associated with them as well as with other typical filtering methods because a large amount of useful biological information can be lost, and there are many trade-offs between various filtering methods. Moreover, conventional filtering cannot always fully address the physicality of the signal-processing problem in terms of extracting specific signals due to particular biological sources of interest such as the stomach, heart and bowel. In this paper, we demonstrate the use of fast independent component analysis (FICA) for the removal of both biological and non-biological artifacts from multi-channel MGG recordings acquired using a superconducting quantum intereference device (SQUID) magnetometer. Specifically, we show that the signal of gastric electrical control activity (ECA) can be isolated from SQUID data as an independent component even in the presence of severe motion, cardiac and respiratory artifacts. The accuracy of the method is analyzed by comparing FICA-extracted versus electrode-measured respiratory signals. It is concluded that, with this method, reliable results may be obtained for a wide array of magnetic recording scenarios.

Keywords: artifact reduction, magnetogastrography, independent component analysis

(Some figures in this article are in colour only in the electronic version)

## 1. Introduction and background

There is significant clinical interest associated with the analysis of gastric and intestinal motility from bioelectric and biomagnetic recordings due to the relationship that has been shown to exist between gastrointestinal (GI) disorders and abnormalities in the characteristics of gastric electrical activity (GEA). In humans, GEA consists of an electrical control activity (ECA) that can be recorded as an electrical slow wave, and an electrical response activity (ERA) that is characterized by spiking potentials during the plateau phase of the ECA.

ECA propagation along the GI tract is mediated by the presence of both circular and longitudinal smooth muscle groups (Bortoff *et al* 1981), which are coupled in healthy subjects (Elden and Bortoff 1984). The interstitial cells of Cajal (ICC) are pacemakers which possess ionic conductances that trigger slow wave activity, whereas smooth muscle cells lack the basic mechanisms required to generate ECA. Cells of the latter type respond to the depolarization and repolarization cycle imposed by the ICC network and regulate L-type $Ca^{2+}$ currents which are also responsible for the contractile behavior of the stomach (Horowitz *et al* 1999). Anatomically, the antral region of the stomach acts as a pacemaker that generates and drives ECA slow waves along the gastric corpus toward the pylorus (Horiguchi *et al* 2001). The ECA signal recorded by the electrogastrogram (EGG) consists of a periodic slow wave that approximates a sinusoid with an approximate frequency of 3 cycles per minute (cpm). The presence of abnormal ECA propagation patterns has been found to be associated with many diseases, including gastroparesis (Smith *et al* 2003), gastric myoelectrical dysrhythmia (Qian *et al* 2003), atrophy and hypertrophy (Bortoff and Sillin 1986) and diabetic gastropathy (Koch 2001).

The electrogastrogram (EGG) and magnetogastrogram (MGG) are the two most important procedures for measuring and quantifying GEA. The EGG signal was first recorded by Alvarez (1921) with a galvanometer; the use of electrodes for this procedure was pioneered by Bozler (1945). Hamilton *et al* (1986) were the first to use EGG with the purpose of investigating gastric motility disturbances from recordings of ECA potentials in humans.

The reliability of EGG has been questioned. Liang and Chen (1997) showed that the detectability of gastric slow wave propagation from cutaneous EGG is dependent on the thickness of the abdominal wall and on the propagation velocity of the serosal slow wave. Bortolotti (1998) pointed out that the practicality of using EGG to detect alterations in slow wave frequency due to tachy- and bradygastria remains problematic in spite of considerable recent progress to improve filtering and analysis methods. Reservations concerning the significance of EGG as a diagnosis tool were also expressed by Camilleri *et al* (1998), who indicated that the precise meaning of dysrhythmias, signal amplitude changes and the duration of such abnormalities relative to gastric emptying as quantified by EGG remain to be clarified. In addition, the stability of EGG recordings is affected by a variety of artifacts, such as the overlap of the electrical activities of the colon and stomach in cutaneous EGG recordings (Amaris *et al* 2002).

In response to these concerns, magnetogastrography (MGG) and magnetoenterography (MENG) were developed as non-invasive alternatives to EGG (Comani *et al* 1996, Staton *et al* 1995, Bradshaw 1995). Bradshaw *et al* (1997) showed that a high degree of correlation exists between the ECA frequency values determined using EGG and MGG (Bradshaw *et al* 1997). EGG signals depend on the conductivities of the tissues where the quasistatic current sources producing them are located; moreover, they also depend on the permittivities of the insulating abdominal layers that are interposed between these current sources and the measurement sensors. Biomagnetic fields, on the other hand, are also dependent on the conductivities of the tissues where their sources are located because current sources are themselves dependent on

conductivity. However, a key aspect to be noted here is that, in the case of the multilayered spheroidal model, magnetic fields depend to a far greater extent on the permeability—rather than permittivity—of the tissues interposed between the sources of these fields and the locations where they are measured. This has been shown by Hämäläinen and Sarvas (1989), where these authors were able to demonstrate that secondary currents on outer interfaces between bioconductors only give negligible contributions to the magnetic field measured from outside the body. Because the conductivity of the tissues where the sources are located affects only these secondary currents, it can be concluded that permittivity affects the measured magnetic fields less than permeability. It should also be mentioned here that the argument of Hämäläinen and Sarvas applies to our case because the multilayered spheroidal model has been found to be appropriate not only for the brain but also for the stomach (Bradshaw *et al* 2001a, 2001b, Irimia and Bradshaw 2005, Irimia 2005). Thus, a distinction arises in this respect between bioelectric and biomagnetic fields in terms of how strongly they depend on the layers of abdominal tissues that are positioned between their sources and the measurement apparatus. Whereas the currents themselves depend on the permittivities of the emitting tissues in both cases, the strength of the magnetic field as measured from the sensor location is affected to a far greater extent by the permeability of the interposed layers than by their permittivity. Because the permeability of these interposed tissues that 'screen out' the field is nearly equal to that of free space (whereas their permittivity is not), it can be argued that there may be significant advantages to the use of MGG for clinical investigations as compared to EGG (Bradshaw *et al* 2001b).

## 2. Motivation and purpose

The artifact removal problem for magnetic fields recorded from GI electrical activity is at least as difficult as it is in electro- (EEG) and magneto-encephalography (MEG) or electro- (ECG) and magneto-cardiography (MCG). In the case of MEG compared to MGG, the head is positioned farther away from other organs that produce strong magnetic fields (such as the heart and abdomen) (Hämäläinen *et al* 1993). In MCG, the magnetic signal of the heart is quite strong compared to that of the surrounding organs, which is beneficial in terms of the signal-to-noise ratios of MCG experiments (Comani *et al* 2004).

The stomach is positioned just below the diaphragm, which implies that respiration artifacts can be very strong if the subject is breathing. In the case of conscious humans, this problem can be partially addressed by asking subjects to hold their breath for specified periods of time (Bradshaw *et al* 1999). This solution is not entirely satisfactory, as it significantly limits the length of data segments. Longer segments can be acquired while the subject is breathing; however, for such data to be easily analyzable, a method is required in order to address the respiratory artifact issue. Thus far, both conventional filtering (Bradshaw *et al* 1997) and adaptive respiration signal subtraction (Palmer 2005) have been implemented for MGG, but only with modest success. Conventional methods—such as Butterworth and Tchebyshev filters—are capable of removing respiration artifacts—albeit imperfectly—but, in doing so, they can also remove important biological information from the data (Nolte and Curio 1999). Adaptive respiration subtraction can be implemented by subtracting a (scaled) respiration signal recorded in a reference sensor from channels that record magnetic data. However, the implementation of this method is problematic—to say the least—in realistic contexts because, while the frequency of the respiration signal recorded by the reference respiration channel may be identical to that recorded by the magnetic data channels, the waveform assumed by the respiration artifact signal can differ greatly across channels, which can make signal subtraction more problematic (Vrba and Robinson 2001).

A major problem of MGG data acquisition is related to the presence of motion artifacts caused by small movements made by subjects in the waking state while data are being acquired. Very often, MGG measurements are made both pre- and post-prandially for periods of time of the order of hours. This is required because certain pathological changes in gastric activity as a result of eating occur only gradually in time, which can require lengthy data acquisition sessions (Parkman *et al* 2003). In view of this, motion artifacts caused by movements of the human subject under the measurement apparatus are often unavoidable.

Another important problem consists of the fact that the gastric ECA signal is often obscured in MGG recordings by the presence of cardiac, muscular and/or intestinal artifacts, which can also reduce the quality of MGG signals. Although cardiac activity usually has its frequency peak between 60 and 80 cpm in resting humans (as opposed to the frequency peak of ECA, which is located around 3 cpm), the power spectrum of the cardiac signal does contain a large amount of energy in the low-frequency range (Cohen 1988), which implies that a certain amount of overlap exists between cardiac and gastric signals. The same can be said about cardiac and intestinal signals because the dominating frequency of the latter is between 8 and 12 cpm, which is also in the range of low-frequency cardiac activity. Finally, the fact that respiration causes motion artifacts implies that SQUID sensors record magnetic field information at different positions with respect to the location of the stomach throughout the data acquisition process. This complicates the issue of applying inverse procedures with accuracy.

In view of the challenges described above, the purpose of this paper is to demonstrate the use of the fast independent component analysis (FICA) technique for the separation of the gastric signal from MGG data in the presence of severe motion, cardiac and respiratory artifacts. In the following section, we describe our experimental data acquisition protocols and present an overview of the implemented FICA algorithm. We continue by illustrating the application of FICA to an experimental MGG data set containing a significant amount of artifacts. In particular, the isolation of the gastric signal as well as that of cardiac, respiratory and other motion artifacts is demonstrated. An accuracy analysis of our results is then carried out to conclude that the method is quite robust and appropriate for the analysis of MGG signals.

## 3. Methods

In our acquisition protocol, MGG signals are recorded using a multi-channel SQUID magnetometer (637i model, Tristan Inc., San Diego, CA) that possesses a set of detection coils located at the bottom of an insulated dewar made of garolite (G10) and aluminum and filled with liquid helium ($T \approx 4$ K). The detection coils are magnetically coupled to the SQUID coils that convert magnetic flux incident on the detection coils to voltage signals that are amplified and then acquired by a digital computer at the rate of 3 kHz. Detection coils are arranged in gradiometer format as a horizontal grid and 19 of them record the Cartesian component of the magnetic field that is normal with respect to the grid plane. At five of the 19 locations, the other two Cartesian components of the field are also measured.

Our studies are approved by the Vanderbilt University Institutional Review Board. Human volunteers are positioned underneath the SQUID magnetometer inside a magnetically shielded room (Amuneal Manufacturing Corp., Philadelphia, PA). Informed consent is obtained from each of these volunteers. Subjects are asked to lie quietly during each recording, which lasts for approximately 30–45 min when pre-prandial data are acquired and for 90–120 min when post-prandial recordings are made. Post-prandial recordings require longer acquisition time frames because some of the physiological processes associated with digestion often last longer than 45 min (Camilleri *et al* 1998). Throughout the recording period, the magnetometer is

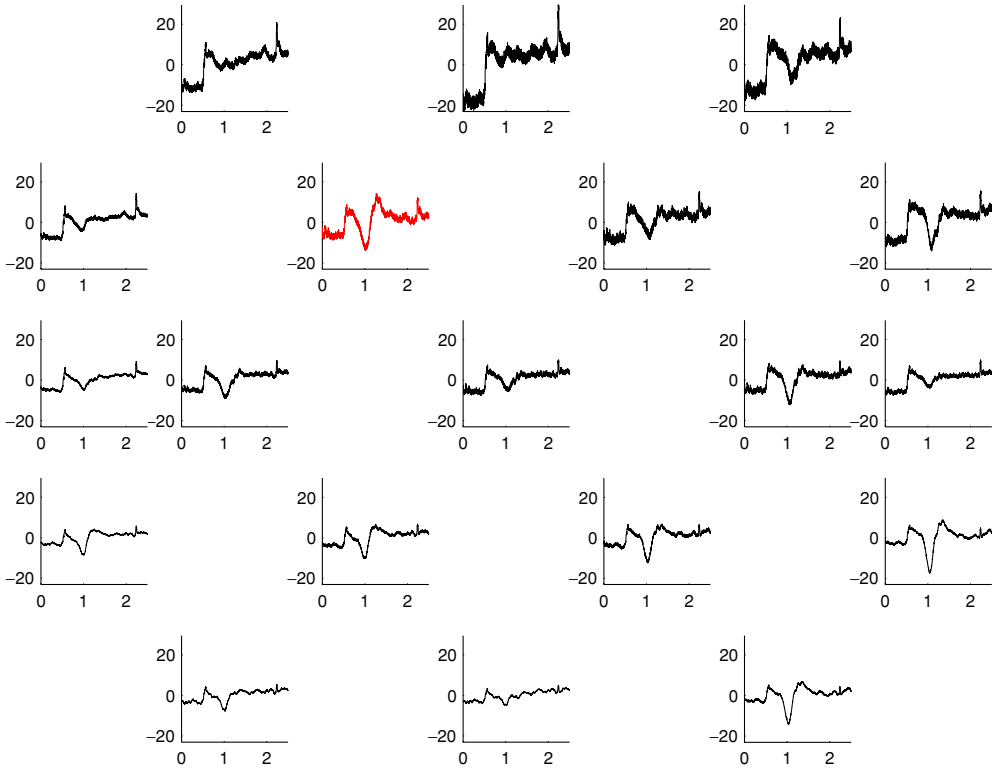

**Figure 1.** Sample raw MGG SQUID recordings ($B_z$ field component signals) acquired from a healthy human patient for a time interval of 2.5 min. Magnetic field values (pT) are plotted against time (min). Plots are shown in the approximate spatial arrangement of the SQUID magnetometer coils. The signal due to the stomach is not apparent from these recordings due to the presence of severe motion, cardiac and respiratory artifacts.

oriented such that the coils measuring the $\hat{\mathbf{x}}$ and $\hat{\mathbf{y}}$ components of the signal tangential to the body surface are oriented in the sagittal and horizontal planes, and the coil measuring the $\hat{\mathbf{z}}$ component normal to the body surface is oriented in the frontal plane. Sample plots of the MGG signals recorded from one healthy subject in which substantial noise and artifact components are present are presented in figure 1.

We have employed fast independent component analysis (FICA) to analyze MGG recordings from ten healthy adult human volunteers. Since ICA involves the computation of the covariance matrix of the MGG data—which can be (near)-singular—data dimensionality is reduced in our approach (Irimia *et al* 2005) using principal component analysis (PCA), thereafter the FICA algorithm described below is applied to the reduced data. PCA is a multivariate analysis technique that attempts to describe the variation of a set of multivariate data in terms of a set of uncorrelated variables, each of which is a particular linear combination of the original variables (Everitt and Dunn 1992). The principal components (PCs) of the MGG observation set are linear combinations of the underlying variables in that set; specifically, they are those particular combinations which maximize the variances of each PC subject to the constraint of orthonormality. The optimization technique of Lagrange multipliers (Morisson 1967, Chatfield and Collins 1980) is used in our case to maximize the variance of each PC, which leads to the calculation of eigenvectors for the variance–covariance matrix of the

original signals. These eigenvectors correspond to the eigenvalues of the variance–covariance matrix arranged in descending order according to their magnitude; thus, the first PC can be interpreted as that linear combination of the original variables which maximally discriminates among a set of subjects. After dimensionality reduction, the number of PCs retained were set to the number of input signals, which account for most of the explained variance in the data.

ICA is a data analysis technique that attempts to recover unobserved signals or 'sources' from observed mixtures, i.e. typically from the output of an array of sensors (Cardoso 1998). ICA has already been employed quite successfully in a variety of fields, including EEG (Makeig *et al* 1996, Makeig *et al* 1997, Jung *et al* 2000), MEG (Vigário *et al* 1996, 2000, Vigario 1997), fetal ECG (de Lathauwer *et al* 2000) and MCG (Comani *et al* 2004). In GI research, ICA was used by Wang *et al* to blindly separate slow waves and spikes from invasive measurements of gastrointestinal electrical activity (Wang and Chen 2001) in animals. It was used by Liang (2005) to extract the ECA waveform from invasive EGG measurements. Our study is the first one to demonstrate the use of ICA for non-invasive MGG gastric signal extraction.

Let $x_1, x_2, \ldots, x_n$ be a set of $n$ observed random variables expressed as linear combinations of another $n$ random variable $s_1, s_2, \ldots, s_n$, i.e.

$$x_i = a_{i1}s_1 + a_{i2}s_2 + \cdots + a_{in}s_n \tag{1}$$

$$= \sum_{j=1}^{n} a_{ij}s_j, \tag{2}$$

where

$$i = 1, \ldots, n \tag{3}$$

$$a_{ij} \in \mathbb{R}. \tag{4}$$

The $s_i$ are assumed to be statistically mutually independent. Let $\mathbf{x}$ and $\mathbf{s}$ denote the random vectors containing the mixtures $x_1, x_2, \ldots, x_n$ and $s_1, s_2, \ldots, s_n$, respectively and let $\mathbf{A}$ denote the matrix with entries $A_{ij} = a_{ij}$. The mixing model above can then be written simply as

$$\mathbf{x} = \mathbf{A}\mathbf{s}. \tag{5}$$

In terms of the formalism provided above, the task involved in ICA consists of finding $\mathbf{s}$ (in our case, the underlying gastric, cardiac, etc signals) in terms of some given $\mathbf{x}$ (i.e., SQUID-recorded signals for our purposes) by identifying a suitable choice of the matrix elements of $\mathbf{A}$. We have used the fixed-point FICA algorithm of Hyvärinen as described by Hyvärinen and Oja (1997). Since the details of this algorithm are extensively discussed elsewhere (Hyvärinen 1999a, 1999b, Hyvärinen and Oja 2000), we only summarize this method here.

Let the differential entropy $H$ of a random vector $\mathbf{y} = (y_1, y_2, \ldots, y_n)^T$ with probability density function $f(\cdot)$ be defined as

$$H(\mathbf{y}) = -\int \mathrm{d}\mathbf{y}\, f(\mathbf{y}) \ln f(\mathbf{y}). \tag{6}$$

In the present case, the term entropy refers to the basic information-theoretic quantity for continuous one-dimensional random variables. The negentropy $J$ can be interpreted as a measure of non-Gaussianity and can be defined as

$$J(\mathbf{y}) = H(\mathbf{y}_g) - H(\mathbf{y}), \tag{7}$$

where $\mathbf{y}_g$ is a Gaussian random vector of the same covariance matrix as $\mathbf{y}$. The mutual information $I$ between the $n$ scalar random variables $y_i$ is a natural measure of the dependence between random variables that can be defined as

$$I(y_1, y_2, \ldots, y_n) = J(\mathbf{y}) - \sum_i J(y_i), \tag{8}$$

where

$$J(y_i) = H(y_{ig}) - H(y_i) \tag{9}$$

since $y_i$ is a *scalar* random variable. The ICA of the random vector $\mathbf{x}$ can now be defined as the invertible transformation $\mathbf{s} = \mathbf{W}\mathbf{x}$ chosen in such a way that $I(s_1, s_2, \ldots, s_n)$ is minimized. This is equivalent to the task of finding the direction in which negentropy is maximized. To achieve this, negentropy is first approximated in our approach using

$$J(\mathbf{w}) = [\mathrm{E}\{G(\mathbf{w}^T\mathbf{x})\} - \mathrm{E}\{G(\nu)\}]^2, \tag{10}$$

where $\mathrm{E}\{\cdot\}$ is the expectation operator, $\mathbf{w}$ is an $m$-dimensional weight vector subject to the constraint $\mathrm{E}\{(\mathbf{w}^T\mathbf{x})^2\} = 1$, $\nu$ is a standardized Gaussian variable and $G$ is the so-called contrast function ($g$ and $g'$ denote the first and second derivatives of $G$). Theoretically, $G$ can be any non-quadratic form; however, three contrast functions are most commonly used, namely

$$G_1(u) = \frac{1}{a_1} \ln\cosh(a_1 u) \tag{11}$$

$$G_2(u) = -\frac{1}{a_2} \exp\left(-\frac{a_2 u^2}{2}\right) \tag{12}$$

$$G_3(u) = \frac{u^4}{4}, \tag{13}$$

where $1 \leqslant a_1 \leqslant 2$ and $a_2 \approx 1$ are constants. Our experience showed that most of the ICs isolated from our MGG data were sub-Gaussian; therefore, of the three functions above, $G_3$ was selected for our calculations because it is very suitable as a general purpose contrast function in such cases (Bell and Sejnowski 1995, Hyvärinen *et al* 1995, Hyvärinen 1999b).

The task of maximizing negentropy can be rephrased as the goal of finding $\max\left\{\sum_i J_G(\mathbf{w}_i)\right\}, i = 1, \ldots, n$, subject to the constraint $\mathrm{E}\left\{\left(\mathbf{w}_j^T\mathbf{x}\right)\left(\mathbf{w}_k^T\mathbf{x}\right)\right\} = \delta_{jk}$, where $\delta_{jk}$ denotes the Kronecker delta function. In our fixed-point approach, after data sphering (whitening) has been performed, each new value of $\mathbf{w}$ (denoted by $\mathbf{w}^+$) is obtained iteratively from the old value of $\mathbf{w}$ (denoted by $\mathbf{w}^-$) using the formulae

$$\mathbf{w}' = \mathrm{E}\{\mathbf{x}g(\mathbf{w}^{-T}\mathbf{x})\} - \mathrm{E}\{g'(\mathbf{w}^{-T}\mathbf{x})\}\mathbf{w}^- \tag{14}$$

$$\mathbf{w}^+ = \frac{\mathbf{w}'}{\|\mathbf{w}'\|}, \tag{15}$$

where $\|\mathbf{w}'\|$ indicates the Euclidian norm of $\mathbf{w}'$ and $\mathbf{w}^{-T}$ indicates the transpose of $\mathbf{w}^-$ (not to be confused with $(\mathbf{w}^{-1})^T$, i.e. the inverse of $\mathbf{w}$ taken to the power $T$). Because our form of the Hyvärinen algorithm makes use of the Newton–Ralphson method of convergence (which is not guaranteed), a stabilizing step is introduced in our approach so as to ensure its convergence.

The expression for the stabilizing step of the algorithm can be derived by making use of the Kuhn–Tucker conditions (Luenberger 1969), according to which the optima of $\mathrm{E}\{G(\mathbf{w}^T\mathbf{x})\}$ under the constraint $\mathrm{E}\{(\mathbf{w}^T\mathbf{x})^2\} = \|\mathbf{w}\| = 1$ are obtained at points where

$$\mathrm{E}\{\mathbf{x}g(\mathbf{w}^T\mathbf{x})\} - \beta\mathbf{w} = 0. \tag{16}$$

The symbol $\beta$ used above denotes the quantity

$$\beta = \mathrm{E}\{\mathbf{w}^{-T}\mathbf{x}g(\mathbf{w}^{-T}\mathbf{x})\}. \tag{17}$$

To solve equation (16) using Newton's method, one can label the left-hand side of the equation above as a function $F$ that must be set to zero. The Jacobian matrix $JF$ of this function can be computed from

$$JF = \mathrm{E}\{\mathbf{x}\mathbf{x}'g'(\mathbf{w}^{T}\mathbf{x})\} - \beta\mathbf{I}, \tag{18}$$

where $\mathbf{I}$ is the identity matrix. Using the set of approximations

$$\mathrm{E}\{\mathbf{x}\mathbf{x}'g'(\mathbf{w}^{T}\mathbf{x})\} \approx \mathrm{E}\{\mathbf{x}\mathbf{x}^{T}\}\mathrm{E}\{g'(\mathbf{w}^{T}\mathbf{x})\} \tag{19}$$

$$\approx \mathrm{E}\{g'(\mathbf{w}^{T}\mathbf{x})\}\mathbf{I}, \tag{20}$$

the Jacobian matrix becomes diagonal and can be inverted. Then, by applying Newton's method, equation (16) yields

$$\mathbf{w}' = \mathbf{w}^{-} - \mu\frac{\mathrm{E}\{\mathbf{x}g(\mathbf{w}^{-T}\mathbf{x})\} - \beta\mathbf{w}^{-}}{\mathrm{E}\{g'(\mathbf{w}^{-T}\mathbf{x})\} - \beta} \tag{21}$$

$$\mathbf{w}^{+} = \frac{\mathbf{w}'}{\|\mathbf{w}'\|}, \tag{22}$$

where $\mu$ is a step size parameter. In our study, the parameter $\mu$ was assigned the value of 0.005. As far as the number of ICs to be separated by FICA is concerned, it was found that a very suitable choice for this was given by the number of SQUID magnetometer channels, i.e. the number of signals acquired during each experiment. Within the theoretical framework of FICA, this choice does have a reasonable amount of merit (Harris 1975) since most of the explained variances of the original signals are accounted for in this approach.

## 4. Results and discussion

The results of our FICA analysis of MGG data are shown in figures 2–5. In figure 2, the ICs isolated with our FICA algorithm are presented. These ICs are arranged from (a) to (h) in the order of their contributions to the variances of the raw SQUID signals. The ones in figures 2(a)–(d) can be identified as motion artifacts caused by the movement of the human subject under the SQUID. These ICs have higher magnitudes than those in figures 2(e)–(h) and in fact dominate the waveforms of the raw SQUID signals shown in figure 1. Because of these artifacts, the waveform of the gastric ECA signal is not distinguishable in the latter plots. Figure 2(e) shows a sinusoidal waveform with a dominating frequency of approximately 3 cpm, corresponding to the gastric signal. The cardiac MCG signal was also isolated by the algorithm as a separate IC with a dominating frequency of about 75 cpm, as shown in figure 2(f). The respiratory artifact in the SQUID data is of smaller magnitude than both the gastric and the cardiac signals and has a dominating frequency of approximately 13 cpm (figure 2(g)). Finally, the FICA algorithm was also found to be capable of isolating a high-frequency IC that we believe to correspond to environmental and magnetometer noise (figure 2(h)), although further study is required for clarification. If FICA is indeed able to obtain a quantitative assessment of noise, the algorithm may be very suitable for measuring the signal-to-noise ratio of MGG experiments.

Some of the ICs in figure 2 can be identified from the raw SQUID data in figure 1; this is demonstrated in figure 3. The most important conclusion that can be drawn from this figure is that, if artifacts due to motion, cardiac and respiratory activities are present, the gastric ECA waveform can be very difficult—if not impossible—to distinguish visually. This, together

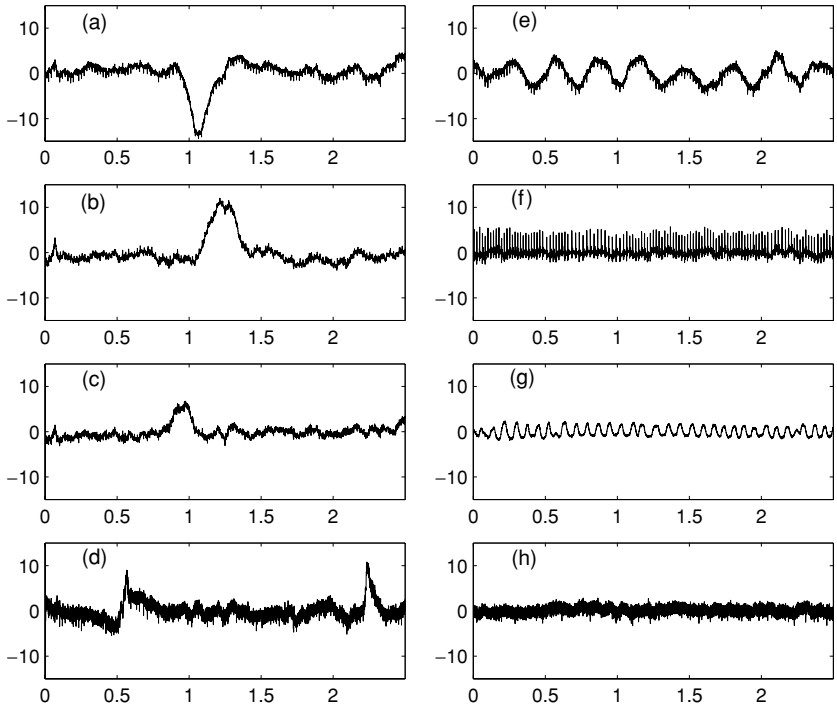


**Figure 2.** ICs obtained from the SQUID data input in figure 1. Magnetic field values (pT) are plotted against time (min). The ICs in (a)–(d) are believed to correspond to (partially overlapping) motion artifacts in the data while (e) shows the gastric slow wave of ECA that was isolated as a separate IC with a dominating frequency of 3 cpm. The ICs corresponding to cardiac activity and to respiration are presented in (f) and (g), respectively. High-frequency noise in the data was also isolated by FICA as a separate IC shown in (h).

with the other results of our study, points out that the FICA algorithm is extremely suitable for the analysis of MGG signals.

Although sometimes difficult, the issues of (1) relating individual ICs to signals produced by actual biological sources and (2) determining realistic polarities and intensities for these signals from ICA information can be addressed in several ways. A common procedure is to retrieve field pattern information from the mixing vector $\mathbf{a}_i$ of the $i$th IC (Vigário *et al* 2000). A spatial mapping technique where mixing vector coefficients are associated with individual spatial locations on the horizontal grid of SQUID channel sensors can then be employed in many cases to determine the sources for which FICA has captured signal information in the ICs. In most cases of interest to our study (including those of gastric or cardiac signals), improved confidence regarding the realism of the IC extraction procedure is provided when ICs have both (1) waveforms that resemble those of biological signals originating in the organs of interest (stomach and heart, in our case) and (2) field patterns that are convincingly associated with the spatial locations of the organs where these biological signals are known to be generated based on *a priori* information. For example, a field pattern revealing the presence of a current dipole in the anatomic region of the gastric corpus and associated with a sinusoidal IC waveform that resembles the gastric ECA signal provides strong indication that the isolated IC corresponds to a signal generated in the stomach. It should be noted that the field patterns discussed here display mappings of dimensionless coefficients in the mixing

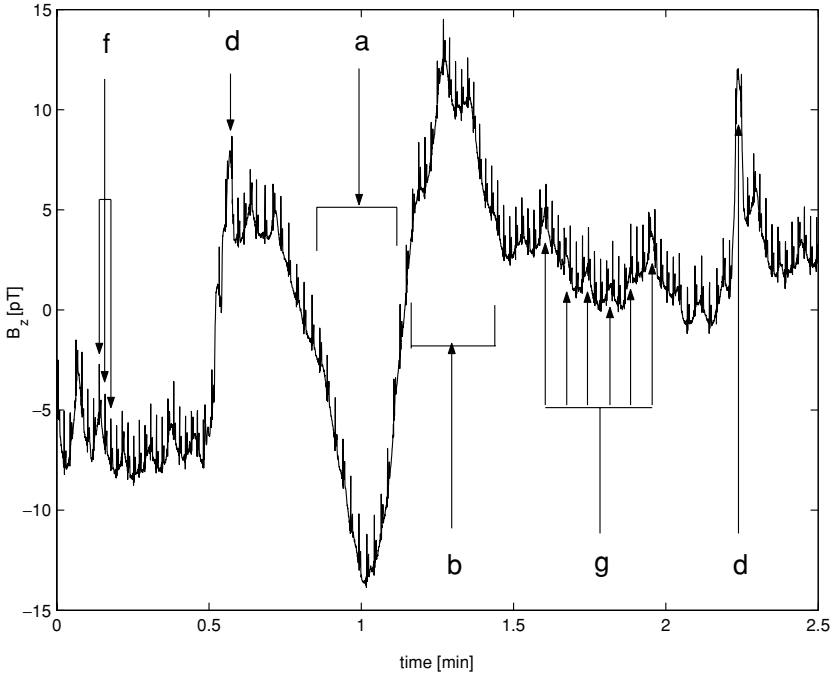


**Figure 3.** Plot of the SQUID signal shown in red (i.e., the signal plotted in the second column and second row) in figure 1. The contributors of each of the ICs separated by FICA in figure 2 are pointed out by arrows. The labels for each arrow correspond to the ICs displayed in the associated subplot of figure 2 that is labeled by the same letter. Thus, the features labeled by (a), (b), (d) are artifacts while those indicated by (f) and (g) are of cardiac and respiratory origin, respectively. The artifact shown in figure 2(c) is not readily apparent due to a cancellation effect between the waveforms due to artifacts (a), (b) and (d). In the cases of cardiac and respiratory activities, only a few selected artifact features are labeled by arrows due to the their large number in the featured plot. Because of these artifacts, the waveform of the signal does not allow one to visually identify the gastric IC of the signal. However, the FICA technique does allow one to do this quite well (see figure 2(e)).

vector $\mathbf{a}_i$ rather than actual magnetic field values. Thus, these visual tools depict the *pattern* of the field associated with a particular IC rather than its actual physical *values*.

An example that illustrates the method of analysis described above is presented in figure 4. There, the field pattern due to the isolated gastric IC in figure 2(e) is displayed. Because the SQUID sensors of the Tristan 637i biomagnetometer are distributed horizontally, the pattern displayed is two- rather than three-dimensional as in the case of MEG, where field patterns are often used (Vigário *et al* 2000). The field pattern in figure 4 reveals the presence of a current dipole oriented in the direction of gastric ECA propagation; the location of the dipole under the measurement grid can be inferred based on a simple geometric argument (Williamson *et al* 1983) which shows that the dipole is located on the line segment that connects the points on the grid where the extrema of the field are located. The approximate orientation of the dipole can then be determined by applying the right-hand rule of electrodynamics. The outline of the stomach is presented solely for illustrative purposes. Aside from being two- rather than three-dimensional, this type of field pattern is very similar to those used in MEG research (Vigário *et al* 2000). What can be inferred from our figure is that the characteristics of the field pattern do satisfy the anatomic (i.e., dipole position) and physiologic (i.e., orientation along the propagation axis) conditions expected for a current dipole that approximates gastric

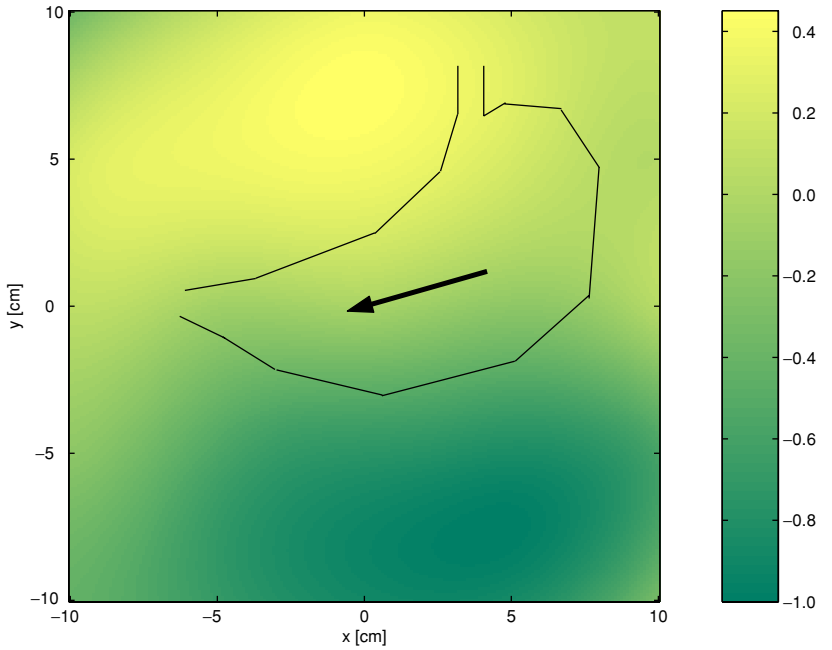


**Figure 4.** Two-dimensional field pattern associated with the gastric IC in figure 2(e). The map was generated by associating the coefficients of the mixing vector $\mathbf{a}_i$ for the gastric IC with the appropriate locations of corresponding SQUID channel sensors. To generate field values for the remaining nodes of the grid where no data had been recorded, two-dimensional biharmonic spline interpolation (Sandwell 1987) was employed. The field pattern values displayed are dimensionless and are normalized for simplicity with respect to $|\max\{\mathbf{a}_i\}|$ (the largest absolute value among the coefficients in the mixing vector of the selected IC). The black arrow indicates the approximate location and projection onto the 2D plane of the gastric current dipole that generates the magnetic field being measured (the orientation of the dipole is determined using the right-hand rule of magnetism). The approximate outline of the stomach is shown for orientation purposes only.

ECA. In conclusion, the field pattern approach—coupled with the visual inspection method for analyzing IC waveforms—does seem to provide conclusive information that can allow us to identify the gastric IC with a reasonable amount of certainty.

Our analysis would be incomplete if it did not offer a measure of FICA accuracy with respect to its ability to recover biological and non-biological signals satisfactorily. To demonstrate the algorithm's ability to extract these ICs faithfully, we show a comparison plot of FICA-reconstructed and electrode-measured respiration activity in figure 5. This figure shows excellent agreement between the reconstructed and the directly measured waveform. The decision to choose this particular type of activity for validation is motivated by the practical ease associated with the non-invasive measurement of respiratory activity. As one may point out, our plot only offers an indirect measure of the accuracy associated with the ability of FICA to reconstruct the gastric IC with high accuracy. To obtain a direct measure of accuracy, an invasive method of validation (e.g., serosal electrode measurements of ECA) would also be required.

The ability of FICA to extract the gastric signal from MGG data can be made more obvious by applying a comparative analysis of this technique to a more traditional method such as digital filtering. A filter that has been widely used in MGG studies is the Butterworth filter (Bradshaw *et al* 1999, 2001b). The second-order Butterworth filter that was used for

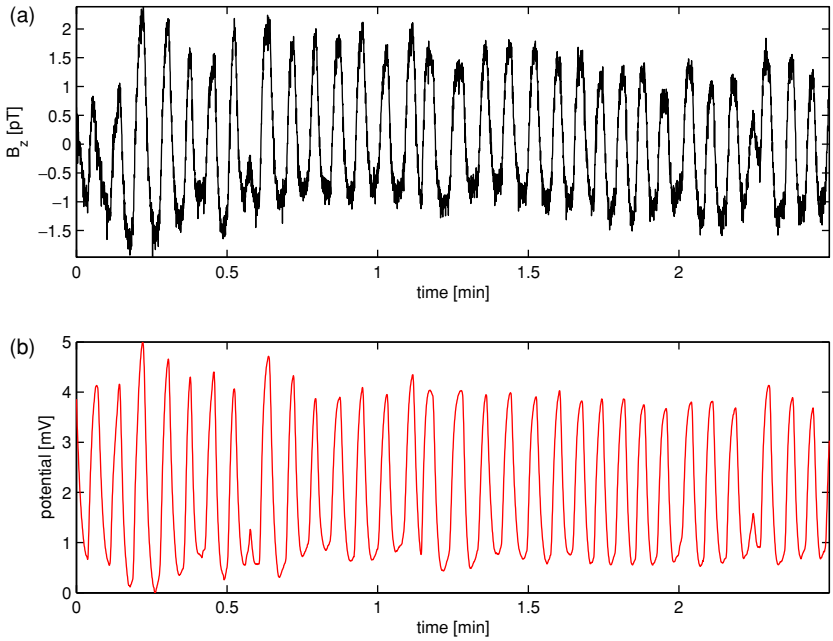


**Figure 5.** Comparison plot of FICA-reconstructed (a) and directly recorded (b) respiration activity. In (a), the plotted respiration signal is the same IC as the one presented in figure 2(g). This IC was reconstructed solely from the data. The signal shown in (b) was directly recorded from the human subject during the experiment using a nasal sensor that records variations in the temperature of the subject's breath. The two plots have different scales and units because the first one is an IC corresponding to a magnetic field component whereas the second one is an electric potential signal that was directly measured with an electrode system. Upon fitting the signal in (a) to the one in (b) in a least-squares sense, the value of the correlation coefficient $r$ between the two quantities was found to be 0.957.

the purpose of our comparison is maximally flat in the pass band and monotonic overall, which reduces the effect of pass band ripples in the signal to a minimum. This type of filter sacrifices rolloff steepness for monotonicity in the pass- and stopbands. To generate the filter, $z$-transform coefficients were created for a lowpass digital Butterworth filter with user-specified cut-off frequencies of 1 and 20 cpm. The low cut-off of 1 cpm was selected in order to eliminate high-frequency noise from the resulting waveform, while the upper cut-off of 20 cpm was chosen so as to take into account the high-frequency components of the gastric signal, whose dominant frequency is 3 cpm. Moreover, the selection of the value for the upper cut-off was motivated by the need to prevent the occurrence of aliasing effects that can appear when filtering windows are too restrictive.

In figure 6, we present the extracted gastric IC as well as the waveform produced as a result of applying the Butterworth filter described above to the SQUID signal drawn in red in figure 1 and reproduced in figure 3. The fact that high-frequency signal components are present in the IC waveform as opposed to the filtered signal waveform is due to the fact that the application of FICA did not involve filtering in any way. One conclusion that can be drawn from figure 6 is that, compared to the filtered signal, the waveform produced by FICA is more similar to the typical gastric ECA signal that has been recorded using both invasive and non-invasive procedures (Bortoff and Sillin 1986, Bradshaw *et al* 2001b). Moreover, there is little similarity between the gastric IC and the filtered signal aside from their comparable magnitudes. The filtered SQUID signal contains a large number of spurious, short-lived oscillations that may

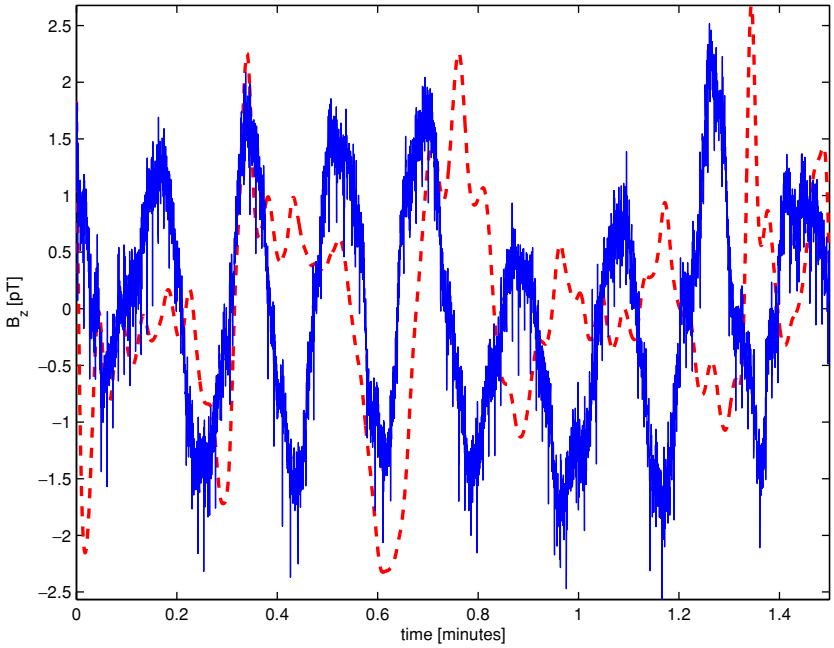


**Figure 6.** Comparison between the gastric IC (blue, continuous) and the filtered SQUID signal in figure 3 after the application of the Butterworth filter (red, dashed). Whereas the magnitude range of the two waveforms is comparable, there are significant differences between the abilities of the two methods to reproduce the expected sinusoidal waveform of the gastric ECA as the latter has been recorded using other procedures (Bortoff and Sillin 1986, Bradshaw *et al* 2001b).

be due to filtering artifacts; its waveform does not exhibit close similarity to the expected sinusoidal shape of the gastric ECA waveform.

Our approach to the use of FICA for the analysis of MGG signals was applied to the data sets acquired from all ten subjects. By employing the methods described in the previous sections, FICA was found to be able to identify the gastric and cardiac signals in all ten subjects. Comparisons between the extracted and the directly measured respiration signals (as shown in figure 5) were also performed for these volunteers, with resulting values for the cross-correlation coefficient $r$ ranging between 0.87 and 0.98; the mean value of $r$ across the volunteers was found to be $r = 0.93 \pm 0.02$ SEM.

## 5. Conclusions and future research

In conclusion, we have demonstrated the use of FICA for the extraction of the gastric ECA signal from artifact-contaminated MGG data. Our analysis was carried out using a fixed-point version of the FICA model with a stabilization constraint imposed for ill-conditioned MGG data. Although the algorithm was shown to extract the respiration activity signal accurately, invasive serosal electrode measurements may be required to directly clarify how powerful the method is for the reconstruction of the gastric ECA signal. Nevertheless, since it is quite probable that such invasive measurements would also be affected by motion artifacts, other types of validation may also be required in cases where such artifacts are also present. The visual analysis of field patterns associated with various ICs was found to be a useful tool in determining the sources of the isolated signals with reasonable certainty. Finally, more

research is required to address the applicability of FICA for the characterization of pathological conditions.

## Acknowledgments

The authors are grateful to L K Cheng (Bioengineering Institute, University of Auckland) and to M A Gallucci (Department of Surgery, Vanderbilt University Medical Center) for their useful comments and suggestions. Funding was provided by the National Institute of Health, grant RO1 DK 58697 and by the Veterans' Affairs Research Service.

## References

Alvarez W C 1921 The electrogastrogram and what it shows *J. Am. Med. Assoc.* **78** 1116–9

Amaris M A, Sanmiguel C P, Sadowski D C, Bowes K L and Mintchev M P 2002 Electrical activity from colon overlaps with normal gastric electrical activity in cutaneous recordings *Dig. Dis. Sci.* **47** 2480–5

Bell A J and Sejnowski T J 1995 An information maximization approach to blind separation and blind deconvolution *Neural Comput.* **7** 1129–59

Bortoff A, Michaels D and Mistretta P 1981 Dominance of longitudinal muscle in propagation of intestinal slow waves *Am. J. Physiol. Cell Physiol.* **240** C135–47

Bortoff A and Sillin L F 1986 Changes in intercellular electrical coupling of smooth muscle accompanying atrophy and hypertrophy *Am. J. Physiol. Cell Physiol.* **250** C292–8

Bortolotti M 1998 Electrogastrography: a seductive promise, only partially kept *Am. J. Gastroenterol.* **93** 1791–4

Bozler E 1945 The action potentials of the stomach *Am. J. Physiol.* **144** 693–700

Bradshaw L A 1995 Measurement and modeling of gastrointestinal bioelectric and biomagnetic fields *PhD Dissertation* Vanderbilt University, Nashville, TN

Bradshaw L A, Allos S H, Wikswo J P Jr and Richards W O 1997 Correlation and comparison of magnetic and electric detection of small intestinal electrical activity *Am. J. Physiol. Gastrointest. Liver Physiol.* **272** G1159–67

Bradshaw L A, Ladipo J K, Staton D J, Wikswo J P Jr and Richards W O 1999 The human vector magnetogastrogram and magnetoenterogram *IEEE Trans. Biomed. Eng.* **46** 959–71

Bradshaw L A, Richards W O and Wikswo J P Jr 2001a Volume conductor effects on the spatial resolution of magnetic fields and electric potentials from gastrointestinal electrical activity *Med. Biol. Eng. Comput.* **39** 35–43

Bradshaw L A, Wijesinghe R S and Wikswo J P Jr 2001b Spatial filter approach for comparison of the forward and inverse problems of electroencephalography and magnetoencephalography *Ann. Biomed. Eng.* **29** 214–26

Camilleri M, Hasler W L, Parkman H P, Quigley E M M and Soffer E 1998 Measurement of gastrointestinal motility in the GI laboratory *Gastroenterology* **115** 747–62

Cardoso J-F 1998 Blind signal separation: statistical principles *Proc. IEEE* **86** 2009–25

Chatfield C and Collins A J 1980 *Introduction to Multivariate Analysis* (London: Chapman and Hall)

Cohen A 1988 *Biomedical Signal Processing* vol 2 (Boca Raton, FL: CRC Press) 121–4

Comani S, Conforto S, di Nuzzo D, Basile M, di Luzio S, Erné S N and Romani G L 1996 Non-invasive detection of gastric myoelectrical activity: comparison between results of magnetogastrography and electrogastrography in normal subjects *Phys. Med.* **12** 35–4

Comani S, Mantini D, Lagatta A, Esposito F, di Luzio S and Romani G L 2004 Time-course reconstruction of fetal cardiac signals from fMCG: independent component analysis versus adaptive maternal beat subtraction *Physiol. Meas.* **25** 1305–21

de Lathauwer L, de Moor B and Vandewalle J 2000 Fetal electrocardiogram extraction by blind source subspace separation *IEEE Trans. Biomed. Eng.* **47** 567–72

Elden L and Bortoff A 1984 Electrical coupling of longitudinal and circular intestinal muscle *Am. J. Physiol. Gastrointest. Liver Physiol.* **246** G618–26

Everitt B S and Dunn G 1992 *Applied Multivariate Data Analysis* (New York: Oxford University Press) pp 45–64

Hämäläinen M S, Hari R, Ilmoniemi R J, Knuutila J and Lounasmaa O 1993 Magnetoencephalography—theory, instrumentation, and applications to noninvasive studies of the working human brain *Rev. Mod. Phys.* **65** 413–97

Hämäläinen M S and Sarvas J 1989 Realistic conductivity geometry model of the human head for interpretation of neuromagnetic data *IEEE Trans. Biomed. Eng.* **36** 165–71

Hamilton J W, Bellahsene B E, Reichelderfer M, Webster J G and Bass P 1986 Human electrogastrograms: comparison of surface and mucosal recordings *Dig. Dis. Sci.* **31** 33–9

Harris R J 1975 *A Primer of Multivariate Statistics* (New York: Academic) pp 156–204

Horiguchi K, Semple G S A, Sanders K M and Ward S M 2001 Distribution of pacemaker function through the tunica muscularis of the canine gastric antrum *J. Physiol.* **537** 237–50

Horowitz B, Ward S M and Sanders K M 1999 Cellular and molecular basis for electrical rhythmicity in gastrointestinal muscles *Annu. Rev. Physiol.* **61** 19–43

Hyvärinen A 1999a Survey on independent component analysis *Neural Comput. Surv.* **2** 94–128

Hyvärinen A 1999b Fast and robust fixed-point algorithms for independent component analysis *IEEE Trans. Neural Netw.* **10** 626–34

Hyvärinen A and Oja E 1997 A fast fixed-point algorithm for independent component analysis *Neural Comput.* **9** 1483–92

Hyvärinen A and Oja E 2000 Independent component analysis: algorithms and applications *Neural Netw.* **13** 411–30

Hyvärinen A, Oja E, Hoyer P O and Hurri J 1995 Image feature extraction by sparse coding and independent component analysis *Proc. Int. Conf. Pattern Recognition (ICPR'98) (Brisbane, Australia)* pp 1268–73

Irimia A 2005 Calculation of the magnetic field due to a bioelectric current dipole in an ellipsoid *J. Phys. A: Math. Gen.* at press

Irimia A and Bradshaw L A 2005 Ellipsoidal electrogastrographic forward modelling *Phys. Med. Biol.* **50** 4429–44

Irimia A, Richards W O and Bradshaw L A 2005 Magnetogastrographic detection of gastric electrical response activity in humans *Am. J. Physiol. Gastrointest. Liver Physiol.* at press

Jung T-P, Makeig S, Humphries C, Lee T-W, McKeown M J, Iragui V and Sejnowski T J 2000 Removing electroencephalographic artifacts by blind source separation *Psychophysiology* **37** 163–78

Koch K L 2001 Electrogastrography: physiological basis and clinical application in diabetic gastropathy *Diabetes Tech. Therap.* **3** 51–62

Liang H 2005 Extraction of gastric slow waves from electrogastrograms: combining independent component analysis and adaptive signal enhancement *Med. Biol. Eng. Comput.* **43** 245–51

Liang J and Chen J D Z 1997 What can be measured from surface electrogastrography—computer simulations *Dig. Dis. Sci.* **42** 1331–43

Luenberger D 1969 *Optimization by Vector Space Methods* (New York: Wiley)

Makeig S, Bell A J, Jung T-P and Sejnowski T J 1996 Independent component analysis of electroencephalographic data *Adv. Neural Inf. Process. Syst.* **8** 145–51

Makeig S, Jung T-P, Bell A J, Ghahremani D and Sejnowski T J 1997 Blind separation of auditory event-related brain responses into independent components *Proc. Natl Acad. Sci. USA* **94** 10979–84

Morisson D F 1967 *Multivariate Statistical Methods* (New York: McGraw-Hill)

Nolte G and Curio G 1999 The effect of artifact rejection by signal-space projection on source localization accuracy in MEG measurements *IEEE Trans. Biomed. Eng.* **46** 400–8

Palmer R L 2005 Characterization of gastric electrical activity using a noninvasive SQUID magnetometer *PhD Thesis* Vanderbilt University

Parkman H P, Hasler W L, Barnett J L and Eaker E Y 2003 Electrogastrography: a document prepared by the gastric section of the American Motility Society Clinical GI Motility Testing Task Force *Neurogastroenterol. Motil.* **15** 89–102

Qian L W, Pasricha P J and Chen J D Z 2003 Origins and patterns of spontaneous and drug-induced canine gastric myoelectrical dysrhythmia *Dig. Dis. Sci.* **48** 508–15

Sandwell D T 1987 Biharmonic spline interpolation of GEOS-3 and SEASAT altimeter data *Geophys. Res. Lett.* **2** 139–42

Smith D S, Williams C S and Ferris C D 2003 Diagnosis and treatment of chronic gastroparesis and chronic intestinal pseudo-obstruction *Gastroenterol. Clin. North Am.* **32** 618–58

Staton D, Golzarian J, Wikswo J P, Friedman R N and Richards W O 1995 Measurements of small bowel electrical activity *in vivo* using a high-resolution SQUID magnetometer *Biomagnetism: Fundamental Research and Clinical Applications* (Boston, MA: Elsevier) pp 748–52

Vigario R N 1997 Extraction of ocular artefacts from EEG using independent component analysis *Electroencephalogr. Clin. Neurophysiol.* **103** 395–404

Vigário R, Jousmäki V, Hämäläinen M, Hari R and Oja E 1996 Independent component analysis for identification of artifacts in magnetoencephalographic recordings *Adv. Neural Inf. Process. Syst.* **10** 229–35

Vigário R, Särelä J, Jousmäki V, Hämäläinen M and Oja E 2000 Independent component approach to the analysis of EEG and MEG recordings *IEEE Trans. Biomed. Eng.* **47** 589–93

Vrba J and Robinson S E 2001 Signal processing in magnetoencephalography *Methods* **25** 249–71

Wang Z S and Chen J D Z 2001 Blind separation of slow waves and spikes from gastrointestinal myoelectrical recordings *IEEE Trans. Inf. Technol. Biomed.* **5** 133–7

Williamson S J, Romani G, Kaufman L and Modena I 1983 Biomagnetism—an interdisciplinary approach *NATO ASI Ser.* **66** 129–39